Journal of Integrative Neuroscience

J. Integr. Neurosci. **2026**; 25(3): 47066
https://doi.org/10.31083/JIN47066

Original Research

Study on the Effects of Transcutaneous Auricular Acupuncture Stimulation of the Vagus Nerve on Post-Traumatic Cerebral Oedema

Yifan Fu[1,2,†], Xiaoxuan Li[1,2,†], Yuanyuan Chen[1,2], Minghao Xu[1,2], Shilin Liu[1,2], Xinyu Xu[1,2], Jiuyu Gao[1,2], Chuandong Cheng[3,4,*], Tao Jiang[1,2,*]

[1]Department of Neurosurgery, The First Affiliated Hospital of Anhui Medical University, 230001 Hefei, Anhui, China
[2]Department of Neurosurgery, Anhui Public Health Clinical Center, 230001 Hefei, Anhui, China
[3]Department of Neurosurgery, The First Affiliated Hospital of University of Science and Technology of China, 230001 Hefei, Anhui, China
[4]Division of Life Sciences and Medicine, University of Science and Technology of China, 230001 Hefei, Anhui, China
*Correspondence: doctorcd@ustc.edu.cn (Chuandong Cheng); jiangtao@ahmu.edu.cn (Tao Jiang)
[†]These authors contributed equally.
Academic Editor: Hongmin Wang
Submitted: 30 September 2025 Revised: 17 December 2025 Accepted: 26 December 2025 Published: 23 March 2026

Abstract

Background: Secondary cerebral oedema following traumatic brain injury (TBI) is a major cause of poor prognosis, primarily driven by neuroinflammation. High-mobility group box 1 (HMGB1) is a key damage-associated molecular pattern that initiates a potent inflammatory cascade, yet targeted pharmacological interventions face clinical translation challenges. Non-invasive transcutaneous auricular vagus nerve stimulation (taVNS) has shown anti-inflammatory potential, but its efficacy and specific mechanisms in treating traumatic cerebral oedema remain unclear. **Methods**: A controlled cortical impact (CCI) model was established in male C57BL/6 mice. The animals were randomly divided into five groups: sham, TBI, TBI + taVNS, TBI + HMGB1 agonist (high glucose), and TBI + HMGB1 antagonist (glycyrrhizic acid). taVNS was administered daily for 7 days. Cerebral oedema volume was quantified via magnetic resonance imaging (MRI) on days 3 and 10 post-injury. Neurological function was assessed using the open field test and modified neurological sign score (mNSS). Molecular mechanisms were investigated through transcriptomic sequencing, enzyme-linked immunosorbent assay (ELISA), western blotting, and immunofluorescence to analyze HMGB1 and downstream inflammatory factors (interleukin-1β (IL-1β), interleukin-6 (IL-6)). **Results**: Transcriptomic analysis revealed that taVNS reversed TBI-induced dysregulation of genes enriched in HMGB1-related pathways (e.g., Ras-associated protein-1 (*Rap1*), mitogen-activated protein kinase (*MAPK*)). Compared with the TBI group, taVNS significantly accelerated the resolution of cerebral oedema (reduction rate: 74.7 $\pm$ 12.1% vs 53.5 $\pm$ 16.2%, $p < 0.05$) and improved neurological function. Mechanistically, taVNS markedly suppressed the upregulation of HMGB1, IL-1β, and IL-6 in both serum and brain tissue. Crucially, the therapeutic effects of taVNS were abolished by HMGB1 agonism (high glucose), while HMGB1 antagonism (glycyrrhizic acid) alone mimicked the benefits of taVNS. **Conclusions**: This study demonstrates that taVNS effectively promotes the resolution of post-traumatic cerebral oedema and facilitates neurological recovery by specifically inhibiting the HMGB1-mediated inflammatory pathway. These findings position taVNS as a promising, non-invasive therapeutic strategy for the early management of secondary brain injury.

Keywords: traumatic brain injury; cerebral edema; vagus nerve stimulation; HMGB1 protein; neuroinflammatory diseases; transcutaneous electric nerve stimulation

1. Introduction

Traumatic brain injury (TBI) represents a significant global public health concern, characterized by high incidence, disability rates, and mortality [1]. The pathology of TBI encompasses two phases: primary and secondary brain injury. Primary brain injury results directly from the impact and is therefore largely untreatable. Within hours to days after the initial mechanical insult, secondary damage evolves into cerebral edema, intracranial hemorrhage, brain swelling, cerebral ischemia, and elevated intracranial pressure [2]. The initial physical impact initiates complex molecular and cellular cascades of secondary injury mechanisms, with cerebral edema being a key factor. Post-traumatic edema is a strong predictor of poor prognosis [3]. Although decompressive craniectomy and osmotic diuretics (e.g., mannitol and hypertonic saline) may temporarily alleviate intracranial hypertension, approximately 35% of patients still experience delayed exacerbation within 72 hours. This fundamentally stems from neuroinflammation-driven blood-brain barrier disruption and glial cell-mediated toxicity [4]. Recent studies indicate that high-mobility group box 1 (HMGB1), released during early neuronal necrosis (2–6 hours post-injury), activates the Toll-like receptor 4 (TLR4)/nuclear factor κB (NF-κB) axis in microglia. This triggers a storm of inflammatory mediators, including interleukin-1β (IL-1β) and interleukin-6 (IL-6), precipitating a malignant transition from vasogenic to cytotoxic edema [5].

HMGB1 is typically expressed in the cell nucleus but may be passively released by necrotic cells or actively secreted by inflammatory cells in response to injury. HMGB1 may also be released from peripheral tissues as part of the systemic inflammatory response, underscoring its broad role in inflammatory processes. Once released, extracellular HMGB1 functions as a damage-associated molecular pattern (DAMP) [6], participating in numerous inflammatory diseases by directly activating receptors, forming complexes with other cytokines, and influencing clearance from the extracellular space [7]. Interventions targeting HMGB1 (e.g., monoclonal antibodies and glycyrrhizic acid) have demonstrated anti-inflammatory potential in animal models. However, clinical translation remains challenging due to low blood-brain barrier penetration (<15%) and risks of systemic immunosuppression. Concurrently, neuromodulation techniques—particularly vagus nerve stimulation (VNS)—have garnered attention for their systemic anti-inflammatory properties.

The vagus nerve, as the tenth cranial nerve, serves as a primary conduit for transmitting biofeedback to the brain [8]. Extensive research indicates that invasive cervical VNS suppresses inflammatory responses by activating the cholinergic anti-inflammatory pathway (CAP). Due to its relative minimal invasiveness and broad applicability, VNS has become one of the most frequently employed neuromodulation techniques [9]. However, the requirement for surgical electrode implantation limits its application in acute cerebral injury. Transcutaneous auricular vagus nerve stimulation (taVNS) emerges as a non-invasive alternative. By stimulating the auricular branch of the vagus nerve in the concha region, it indirectly mimics the therapeutic effects of VNS, offering a novel strategy for modulating inflammation. Presently, the clinical indications for taVNS resemble those of VNS, as supported by previous studies [10,11]. Nevertheless, such research has predominantly focused on epilepsy and depression, leaving the temporal control mechanisms and optimal parameter protocols for traumatic brain injury largely unexplored. Therefore, this study aims to evaluate the therapeutic potential of taVNS in TBI. We sought to determine the therapeutic efficacy of taVNS for traumatic cerebral edema, and to elucidate the pathways and molecular mechanisms through which taVNS modulates brain injury, using HMGB1 agonists and inhibitors for mechanistic validation.

2. Materials and Methods

2.1 Animals

This study employed male SPF (Specific Pathogen Free) C57BL/6 mice (Hefei Jisai Biotechnology Co., Ltd., Heifei, Anhui, China) aged 8–12 weeks, each housed individually for one week prior to experimentation. Mice were maintained under a 12-hour light-dark cycle at 25–26 °C and 50 ± 5% relative humidity with free access to chow and water. Ventilation rates were maintained at 8–15 air changes per hour, and all mice were fed standard irradiated chow.

2.2 Controlled Cortical Impact (CCI) Model Construction

Using a desktop animal anaesthesia ventilator system (Ruiwode Life Sciences Co., Ltd, Hefei, Anhui, China), set the isoflurane concentration to 4%, with a N_2O to O_2 ratio of 2:1 with an oxygen flow rate of 0.5–1 L/min. Place the mouse in the induction box for anaesthetic induction. Observe the mouse until loss of righting reflex is confirmed, then position it on the CCI impactor workbench (YHKJCI990313, Wuhan YiHong Sci.&Tech. Co., Ltd., Wuhan, Hubei, China) and secure it. Connect the inhalation anaesthesia mask (set to 2.5% isoflurane concentration) and maintain body temperature using a heated pad. The scalp hair was removed from the mouse's cranial region. Following alcohol disinfection, the scalp was incised to expose the skull. A square bone window measuring 3–4 mm in diameter was created in the right cerebral hemisphere (2 mm posterior to the anterior fontanelle, 2 mm right of the sagittal line) using a cranial drill, exposing the intact dura mater. Subsequently, employ a 3mm impactor to strike the brain tissue according to pre-set parameters (velocity: 4.5 m/s, depth: 2 mm, dwell time: 200 ms), inducing CCI. Following modelling completion, suture the wound site. After disinfection with povidone-iodine, administer antibiotics via intraperitoneal injection. Upon anaesthetic recovery, transfer the animal to a mouse cage.

2.3 Experimental Groups

Following one week of adaptive feeding, mice were randomly assigned to five groups (n = 15 per group): (1) Sham group (cranial window opened without brain tissue impact), (2) TBI group, (3) TBI + taVNS group, (4) TBI + taVNS + Agonist group (receiving intraperitoneal injection of 50% glucose solution at 6 g/kg/day for 7 consecutive days starting 3 days post-surgery), (5) TBI + Inhibitor group (intraperitoneal injection of glycyrrhizic acid dissolved in 5% DMSO + physiological saline at 50 mg/kg/day for 7 consecutive days starting 3 days post-surgery). For the sake of brevity, the 'TBI + taVNS + Agonist' group is hereafter referred to as the 'Agonist' group, and the 'TBI + Inhibitor' group as the 'Inhibitor' group in the text and figures. The experimental timeline is illustrated in Fig. 1.

2.4 Transcutaneous Auricular Vagus Nerve Stimulation (taVNS)

The taVNS stimulation parameters for this experiment were established based on prior research. The apparatus employed a vagus nerve electrical stimulator (YJT1-240710002) manufactured by Hangzhou Yijian Technology (Hangzhou, Zhejiang, China). To ensure mice could tolerate prolonged vagus nerve electrical stimulation, a benchtop animal anaesthesia ventilator (Ruiwode Life Sciences

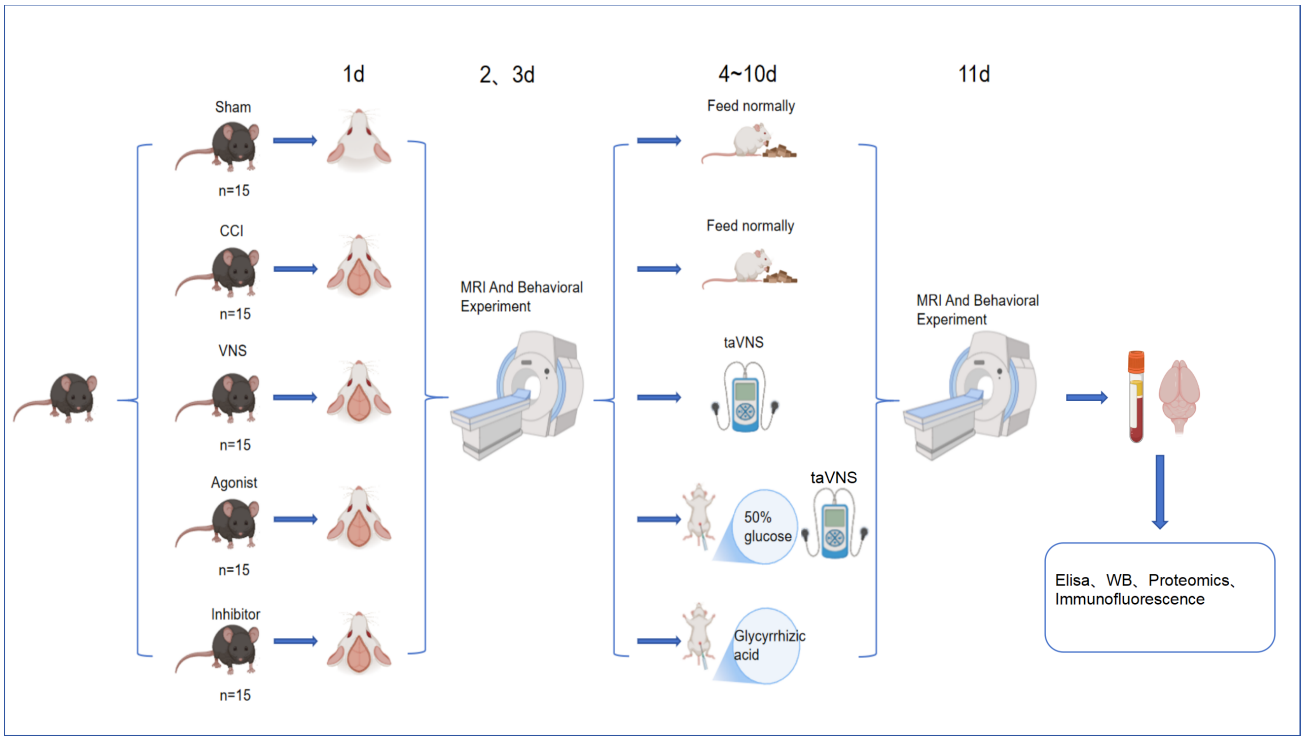

Fig. 1. Experimental timeline and group design. Mice (n = 15/group) were divided into five groups: Sham, CCI, VNS, Agonist + VNS, and Inhibitor. Except for the Sham group, all animals were subjected to CCI. The experimental timeline was as follows: CCI modelling → Behavioral tests and MRI scanning (POD 2) → 7-day intervention → Repeated behavioral tests and MRI scanning → Sample collection. CCI, controlled cortical impact; VNS, vagus nerve stimulation; MRI, magnetic resonance imaging; taVNS, transcutaneous auricular vagus nerve stimulation; WB, western blot; POD 2, Post-Operative Day 2.

Co., Ltd.) was employed. Mice were placed in an induction chamber and anaesthetised with 2% isoflurane (0.5%–1% oxygen) to achieve and maintain anaesthesia. Both auricles were swabbed with alcohol. Electrodes were secured to both auricles, and electrical stimulation commenced. Parameters were set as follows: 0.5 mA, 30 Hz, 30 minutes daily, with 30-second on-intervals followed by 4.5-minute off-intervals. Stimulation was administered daily between 21:00 and 22:00 for a total of 7 days.

2.5 Magnetic Resonance Imaging (MRI)

The experiment employed a Bruker Biospec 9.4T small animal magnetic resonance imaging system (Bruker Biospec MRI, Ettlingen, Germany) with a 20 mm mouse-specific brain coil. Under 4% isoflurane induction anaesthesia (maintained at 1.5%), axial T2-weighted imaging was performed on days 3 and 10 post-TBI surgery (Parameters: repetition time/echo time (TR/TE) = 3272/48 ms, rapid acquisition with relaxation enhancement (RARE) factor = 8, acquisition runs = 3, matrix = 256 × 256, slice thickness = 0.7 mm, 20 consecutive slices covering the entire brain). Throughout scanning, mouse body temperature was maintained at 37.0 ± 0.5 °C via a thermostatic system, with physiological gating synchronised to respiratory movements. Raw images were preprocessed using ITK-SNAP (v3.8.0, https://www.itksnap.org/pmwiki/pmwiki.php?n=Downloads.SNAP3). Edematous regions were semi-automatically segmented based on signal intensity thresholds (>2× mean of contralateral normal brain tissue), with manual refinement to exclude vascular and artefact interference. Volume changes and change rates at both time points were calculated.

2.6 Transcriptomics Analysis

Brain tissue samples were collected from mice in the taVNS group, TBI group, and control group (n = 3 per group). Sequencing analysis was performed using the DNBSEQ platform (https://www.mgi-tech.com/DNBSEQ-Technology.html). Key modules were screened for core pathways via Kyoto Encyclopedia of Genes and Genomes/Gene Ontology (KEGG/GO) enrichment analysis (ClusterProfiler). Target specificity validation was conducted using western blot and enzyme-linked immunosorbent assay (ELISA) cross-platform validation for HMGB1 and its upstream/downstream molecules (including IL-6 and IL-1β).

2.7 Behavioural Science

The experiment employed a standardised open field apparatus (40 cm × 40 cm × 40 cm, opaque black

polypropylene construction, with the central area defined as a 20 cm × 20 cm square) for behavioural assessment on days 2 and 11 post-surgery. Thirty minutes prior to testing, mice were acclimatised to the behavioural laboratory environment (illuminance 50 lux, background noise <45 dB, temperature 22 ± 1 °C). During testing, individual mice were placed in the centre of the open field. An overhead camera (Noldus EthoVision XT 15.0, https://www.noldus.com.cn/ethovision-xt/) continuously recorded spontaneous activity for 5 minutes, analysing the distance travelled within the central square.

2.8 Enzyme-Linked Immunosorbent Assay

The experiment employed an ELISA to detect concentrations of HMGB1 and IL-6 in mouse serum. The mouse HMGB-1 ELISA detection kit (Lianke Bio, SEKM-0032, Shenzhen, Guangdong, China; detection range 15.6–1000 pg/mL, sensitivity 4.7 pg/mL) and the mouse IL-6 ELISA Detection Kit (EMC004, NeoBioscience Technology Co., Ltd., Shenzhen, Guangdong, China; detection range 7.8–500 pg/mL, sensitivity 2.3 pg/mL).

At the end of the experiment, all animals were deeply anesthetized with 3% isoflurane delivered via an inhalation chamber (0.5 L/min oxygen flow) until loss of the righting and pedal withdrawal reflexes. Once deep anesthesia was achieved, the animals were humanely euthanized by cervical dislocation to ensure death, in accordance with the AVMA Guidelines for the Euthanasia of Animals (2020). Whole blood was collected via ocular puncture. After standing for 30 minutes, serum was separated by centrifugation at 3000 ×g for 10 minutes at 4 °C. Aliquoted samples were stored at –80 °C until testing. Prior to assay, samples were thawed and diluted according to kit specifications (HMGB1: 1:20; IL-6: 1:10). Standard dilutions were incubated concurrently with samples (100 µL/well, 37 °C for 90 minutes). Following washing, the following reagents were sequentially applied: biotinylated antibody (1:1000, 37 °C for 60 minutes), streptavidin-HRP (1:2000, 37 °C for 30 minutes), and TMB chromogenic substrate (protected from light for 15 minutes). The reaction was terminated with 2M H_2SO_4 and read at dual wavelengths (450 nm/630 nm) using a microplate reader (BioTek Synergy H1, BioTek Instruments, Winooski, VT, USA).

2.9 Western Blot (WB)

Experimental samples comprised mouse brain tissue perfused and fixed with 4% paraformaldehyde (BL539A, Hefei Biosharp Biotechnology Co., Ltd., Hefei, Anhui, China), rapidly frozen in liquid nitrogen and stored at –80 °C for subsequent analysis. Protein samples (approximately 20 µg per well) were denatured in loading buffer and subjected to electrophoresis on a precast polyacrylamide gel (concentration gel: 80 V for 20 minutes; separation gel: 120 V for 60 minutes). Proteins were subsequently transferred to Polyvinylidene Fluoride (PVDF) membranes (Beyotime, Shanghai, China) using a semi-dry transfer method (PVDF membranes were activated with methanol prior to transfer; both gel and membrane were equilibrated in ice-cold transfer buffer). Transfer conditions were 25 V for 30 min (Buffer: 48 mM Tris, 39 mM glycine, 0.04% SDS, 20% methanol). The membrane was blocked with 5% skimmed milk powder (or bovine serum albumin [BSA] for phosphorylated proteins) at room temperature for 1 hour or overnight at 4 °C. It was then incubated sequentially with specific primary antibodies (glyceraldehyde-3-phosphate dehydrogenase (GAPDH, 1:8000, 60004-1-Ig, Proteintech Group, Inc., Rosemont, IL, USA); HMGB1 (1:1000, ab18256, abcam, Cambridge, UK); IL-1β (1:1000, 12242, Cell Signaling Technology, Danvers, MA, USA); p-NF-κB p65 (1:5000, AF3387, Affinity, Cincinnati, OH, USA); p-ERK1/2 (1:5000, AP0974, Abclonal, Woburn, MA, USA), incubated at room temperature for 2 hours or overnight at 4 °C) and the corresponding HRP-labelled secondary antibody (1:5000, ZB-2305 and AB-2301, Beijing YunTai Bio-Technology Co., Ltd. Beijing, China). Thorough washing with TBST (P1020, Solarbio, Beijing, China) was performed between each antibody incubation step. Target proteins were ultimately visualised using ECL chemiluminescent reagents (WBKLS0100, Millipore, Burlington, MA, USA), with signals captured on an imaging system (NIKON DS-U3, Nikon Corporation, Tokyo, Japan). Exposure time was optimised according to band intensity.

2.10 Immunofluorescence

Mouse brain tissue was perfused and fixed with 4% paraformaldehyde, followed by gradient dehydration and embedding in paraffin. Coronal sections (5 µm thickness) were prepared using a rotary microtome (Leica RM2016; Leica Microsystems (Shanghai) Trading Co., Ltd., Shanghai, China). Deparaffinization and rehydration were performed by sequential immersion in xylene (10023418, Sinopharm, Beijing, China, three changes, 10 min each) and a graded ethanol series (100%, 100%, 95%; 5 min each), followed by a final rinse in distilled water.

Antigen retrieval was carried out by heating the sections in sodium citrate buffer (C1013, Solarbio, 10 mM sodium citrate, 0.05% Tween 20 (ST825, Beyotime, Shanghai, China), pH 6.0) using a pressurized decloaking chamber for 3 minutes. Sections were allowed to cool naturally to room temperature. After washing with PBS, sections were permeabilized with 0.1% Triton X-100 in PBS for 20 minutes at room temperature and then blocked with 3% BSA for 30 minutes at room temperature to prevent non-specific binding.

Sections were incubated overnight at 4 °C in a humidified chamber with the following primary antibodies diluted in PBS: rabbit anti-HMGB1 (1:100, 10829-1-AP, Proteintech Group) and rabbit anti-IL-6 (1:100, 83747-5-RR, Proteintech Group). After thorough washing with PBS (3 × 5 minutes), sections were incubated with an AF488-

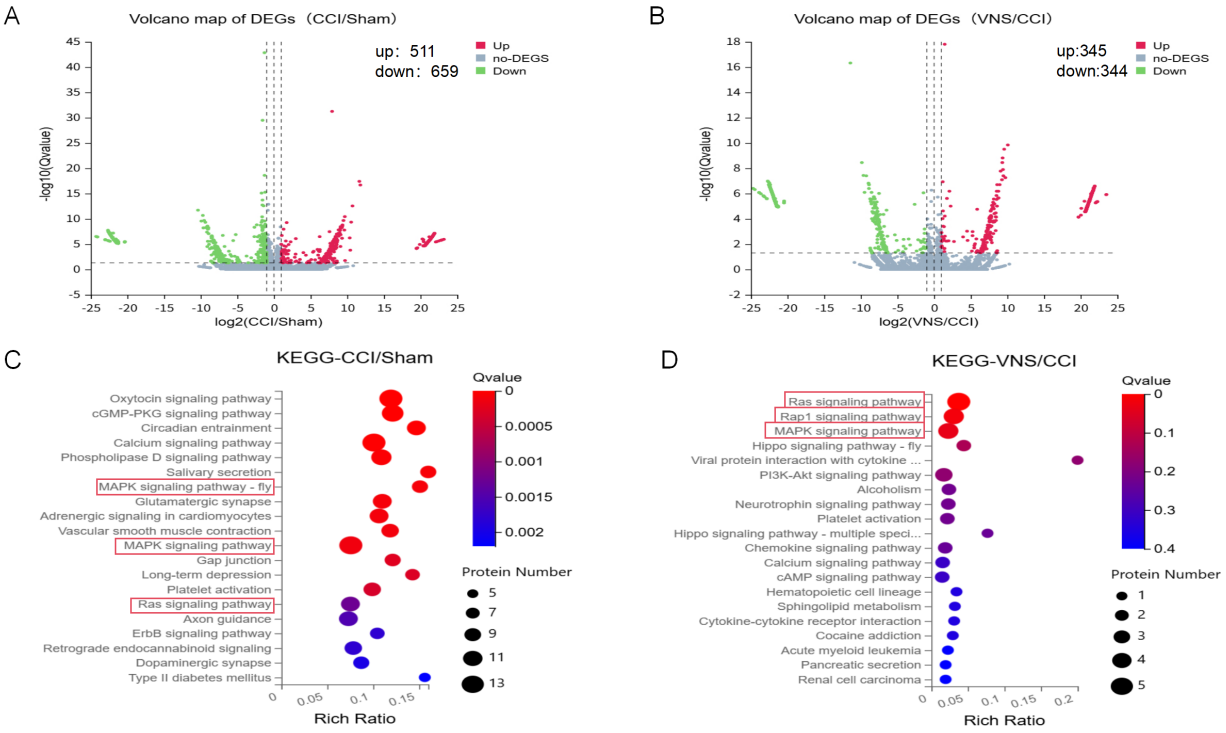

Fig. 2. Transcriptome analysis image. (A) DEGs in CCI versus Sham (volcano plot). (B) DEGs in VNS versus CCI (volcano plot). (C) Pathway enrichment of CCI-upregulated genes identifies HMGB1 signaling as a key upregulated node. (D) Pathway enrichment of VNS-downregulated genes confirms HMGB1 signaling as a primary target for reversion. DEGs, differentially expressed genes; KEGG, Kyoto Encyclopedia of Genes and Genomes; cGMP, cyclic guanosine monophosphate; PKG, protein kinase G; PI3K-Akt, phosphoinositide 3-kinase–protein kinase B signaling pathway; cAMP, cyclic adenosine monophosphate; MAPK, mitogen-activated protein kinase; HMGB1, high-mobility group box 1.

conjugated goat anti-rabbit IgG (H + L) secondary antibody (A0423, 1:500, Beyotime) for 50 minutes at room temperature in the dark. Nuclei were counterstained with 4′,6-diamidino-2-phenylindole (DAPI, Beyotime, C1005) for 10 minutes at room temperature, protected from light.

Finally, the sections were washed with PBS, briefly air-dried, and mounted with an anti-fade mounting medium (P0126, Beyotime). Images were captured using a fluorescence microscope (Nikon Eclipse E100, Shanghai, China) at 400× magnification. Nuclei stained with DAPI appeared blue, while positive signals for HMGB1 and IL-6 were visualized as green fluorescence.

2.11 mNSS Score

The modified neurological sign score (mNSS) was assessed blindly by two researchers, who were completely unaware of the experimental groups and treatments, on postoperative days 2 and 11, respectively. The scoring system encompasses four dimensions: motor function (limb symmetry, crawling ability), sensation (tactile/pain reflexes), balance (balance beam walking, righting reflex), and abnormal behaviour (tremors, circling). The total score ranges from 0 to 18 points (0 = no deficit, 18 = severe deficit). Prior to assessment, mice were acclimatised for 30 minutes in a quiet environment (25 ± 1 °C, light intensity 30 lux). Each test was repeated three times, with the mean value recorded. Non-specific behaviours resulting from anaesthesia or surgical trauma (e.g., incision pain reflex) were excluded.

3. Results

3.1 Transcriptomic Analysis

Transcriptomic analysis revealed 1170 differentially expressed genes in the CCI group, comprising 511 upregulated and 659 downregulated genes. taVNS, the number of differentially expressed genes decreased to 929, including 455 upregulated and 474 downregulated genes. KEGG enrichment analysis confirmed that HMGB1-related pathway genes, such as Rat sarcoma (*Ras*) and mitogen-activated protein kinase (*MAPK*), were significantly enriched among the upregulated genes in the CCI group. Moreover, VNS, HMGB1-related pathway genes, including Ras-related protein 1 (*Rap1*), *Ras*, and *MAPK*, were markedly enriched among the downregulated genes in the VNS group compared to the CCI group (Fig. 2). Preliminary transcriptomic findings suggest that taVNS may regulate HMGB1 levels and inflammation by modulating HMGB1-associated pathways.

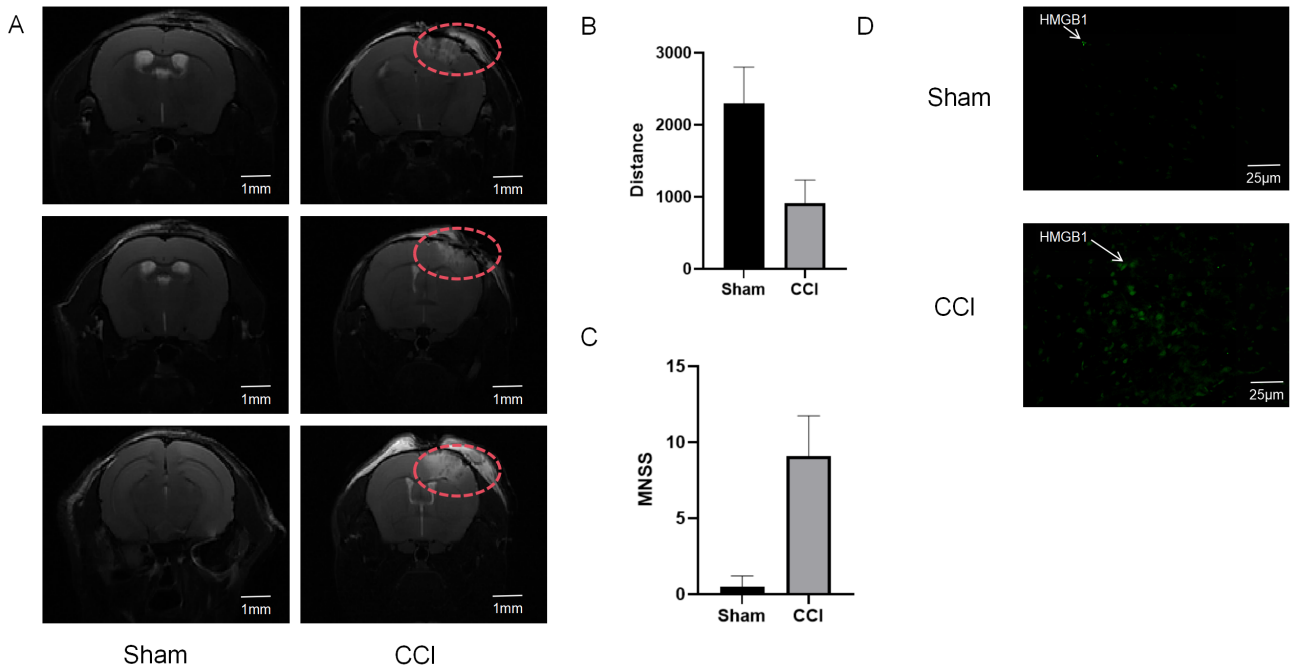

Fig. 3. Successful establishment of the CCI model in mice. (A) Representative MRI images of the brain from the Sham and CCI groups at 3 days post-surgery, showing the distinct lesion area (The area outlined in red dashed lines). Scale bar = 1 mm. (B) Quantitative analysis of the distance traveled in the center of the open field, demonstrating reduced exploratory behavior in the CCI group compared to the Sham group. (C) mNSS scores assessed at 3 days post-surgery, indicating significant neurological deficits in the CCI group. (D) Representative immunofluorescence images showing enhanced expression of HMGB1 (green) in the CCI group compared to the Sham group. Cell nuclei were counterstained with DAPI. Scale bar = 25 μm. mNSS, modified neurological sign score; DAPI, 4′,6-diamidino-2-phenylindole.

3.2 Analysis of the Validity of Models

Magnetic resonance imaging revealed marked cerebral edema in the group compared to the control group at days (Fig. 3A). Combined with analysis, this indicated significant neurological deficits in the group at day 3 distance travelled in the central zone of the open field test decreased by 60% compared to controls (915.20 ± 318.59 cm vs 2296.87 ± 505.15 cm, $p < 0.0001$, Fig. 3B), and the mNSS increased to 9.10 ± 2.64 points (control group 0.50 ± 0.69 points, $p < 0.0001$, Fig. 3C). At the molecular level, the traumatic group exhibited significantly higher serum concentrations of HMGB1 (1325.40 ± 202.64 vs 795.78 ± 433.77 pg/mL; $p = 0.0409$) and IL-6 (76.16 ± 10.35 vs 46.74 ± 19.29 pg/mL; $p = 0.0088$) compared to the control group. Western blot analysis revealed that the expression of HMGB1 protein was 3.7-fold higher, and that of IL-1β was 2.8-fold higher, compared to the control group (both $p < 0.0001$). Using immunofluorescence, we further observed that HMGB1-positive signals (green fluorescence) were significantly increased in the traumatic group compared to the control group (Fig. 3D). The aforementioned multidimensional data consistently confirmed the successful establishment of the model.

3.3 Resolution of Cerebral and Restoration of Neurological Function

ITK-SNAP three-dimensional reconstruction revealed that the taVNS group exhibited a significant reduction in cerebral volume of 74.7 ± 12.1% at 10 days compared to 3 days the trauma group demonstrated only natural absorption of 53.5 ± 16.2% ($p = 0.024$, Fig. 4E), the central area traversed by the taVNS group at 10 days recovered to 76.3% of the control group level (1753.97 ± 588.97 cm vs 915.20 ± 318.59 cm in the trauma group, $p = 0.0031$, Fig. 4A), while the mNSS score decreased to 2.58 ± 1.31 points (group: 9.10 ± 2.64 points, $p < 0.0001$, Fig. 4B). Molecular analysis showed that the taVNS group resulted in a significant reduction in serum HMGB1 levels (853.39 ± 145.94 pg/mL) compared to the traumatic group (1325.40 ± 202.64 pg/mL; $p = 0.0427$). Similarly, serum IL-6 levels were also significantly lower in the taVNS group (47.83 ± 12.64 pg/mL) than in the traumatic group (76.16 ± 10.35 pg/mL; $p = 0.0052$). The protein expression of HMGB1 in brain tissue was reduced to a level 1.5 times that of the control group (compared to 3.7-fold in the trauma group, $p = 0.0003$), while IL-1β levels were downregulated to 1.4-fold (compared to 2.82-fold in the trauma group, $p = 0.0004$) (Fig. 4D, the original WB images can be found in the **Supplementary Materials**). Immunofluorescence revealed that taVNS reversed - induced HMGB1 levels (Fig. 5). These findings

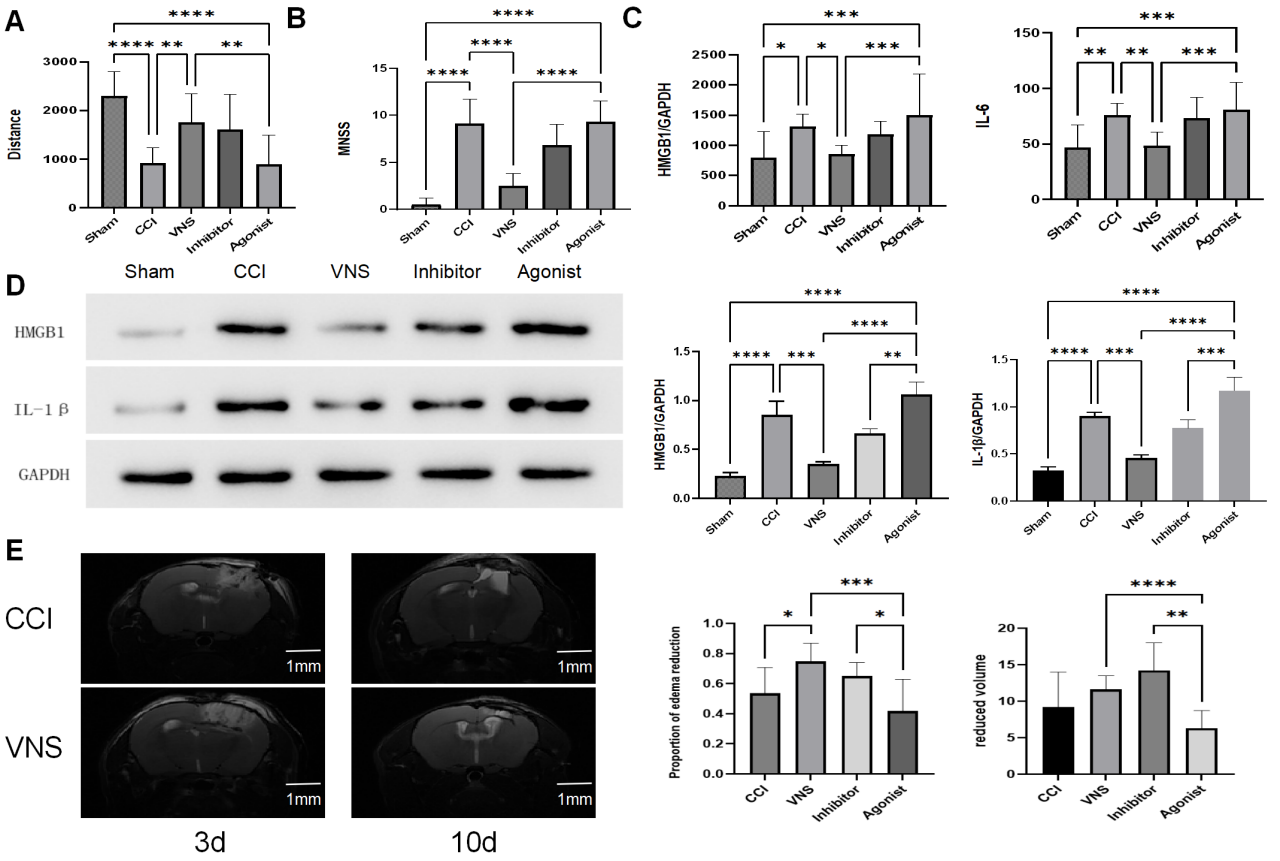

Fig. 4. taVNS improves functional recovery, suppresses neuroinflammation, and promotes edema resolution post-TBI. (A) Analysis of the distance traveled in the center of the open field for all five experimental groups. (B) mNSS neurological scores across all five groups. (C) Serum levels of HMGB1 and IL-6 were quantified by ELISA in the five groups. (D) Protein expression levels of HMGB1 and IL-1β in brain tissue were detected by western blot. The blots for HMGB1, IL-1β, and the loading control GAPDH are displayed. Representative images from three independent experiments are shown. (E) Left: Representative MRI images comparing the CCI and VNS groups after the 7-day intervention, demonstrating enhanced edema resolution with VNS. Scale bar = 1 mm. Right: quantitative analysis of cerebral edema from the four TBI groups, showing the edema volume reduction rate (left graph) and the absolute volume of edema resolved over 7 days (right graph). Data are presented as mean $\pm$ standard deviation (SD). *$p < 0.05$, **$p < 0.01$, ***$p < 0.001$, ****$p < 0.0001$ (by one-way ANOVA with Tukey's post-hoc test). TBI, traumatic brain injury; GAPDH, glyceraldehyde-3-phosphate dehydrogenase; IL-1β, interleukin-1β.

confirm that taVNS accelerates resolution and neural functional by suppressing HMGB1-driven inflammation.

3.4 The HMGB1 Pathway Specifically Mediates the Anti-Edema Effect of taVNS.

3.4.1 taVNS Inhibits the Activation of HMGB1 Downstream Signaling Pathways

To substantiate that the HMGB1 pathway specifically mediates the anti-edema effects of taVNS, we specifically examined the phosphorylation levels of its key downstream effector molecules, NF-κB p65 and ERK1/2, by western blot analysis to directly assess the activation status of these pathways. As illustrated in Fig. 6 (the original WB images can be found in the **Supplementary Materials**), the levels of phosphorylated NF-κB p65 (p-NF-κB p65, Ser536) and phosphorylated ERK1/2 (p-ERK1/2, Thr202/Tyr204) were significantly upregulated in the brain tissue of the CCI group compared to the Sham group (p-NF-κB p65: $p = 0.0002$; p-ERK1/2: $p = 0.0072$), indicating effective activation of the HMGB1-downstream inflammatory signaling after trauma. Crucially, taVNS treatment markedly suppressed this injury-induced phosphorylation (p-NF-κB p65 in taVNS vs CCI: $p = 0.0018$; p-ERK1/2 in taVNS vs CCI: $p = 0.0181$). To establish the specificity of this inhibitory effect, we further employed pharmacological interventions: the co-administration of the HMGB1 agonist (high glucose) with taVNS completely reversed the suppressive effect of taVNS on both p-NF-κB p65 and p-ERK1/2 (p-NF-κB p65 in the Agonist group vs the taVNS group: $p = 0.002$; p-ERK1/2 in the Agonist group vs the taVNS group: $p = 0.0161$). Conversely, the HMGB1 inhibitor (glycyrrhizic acid) alone mimicked the effect of taVNS, significantly re-

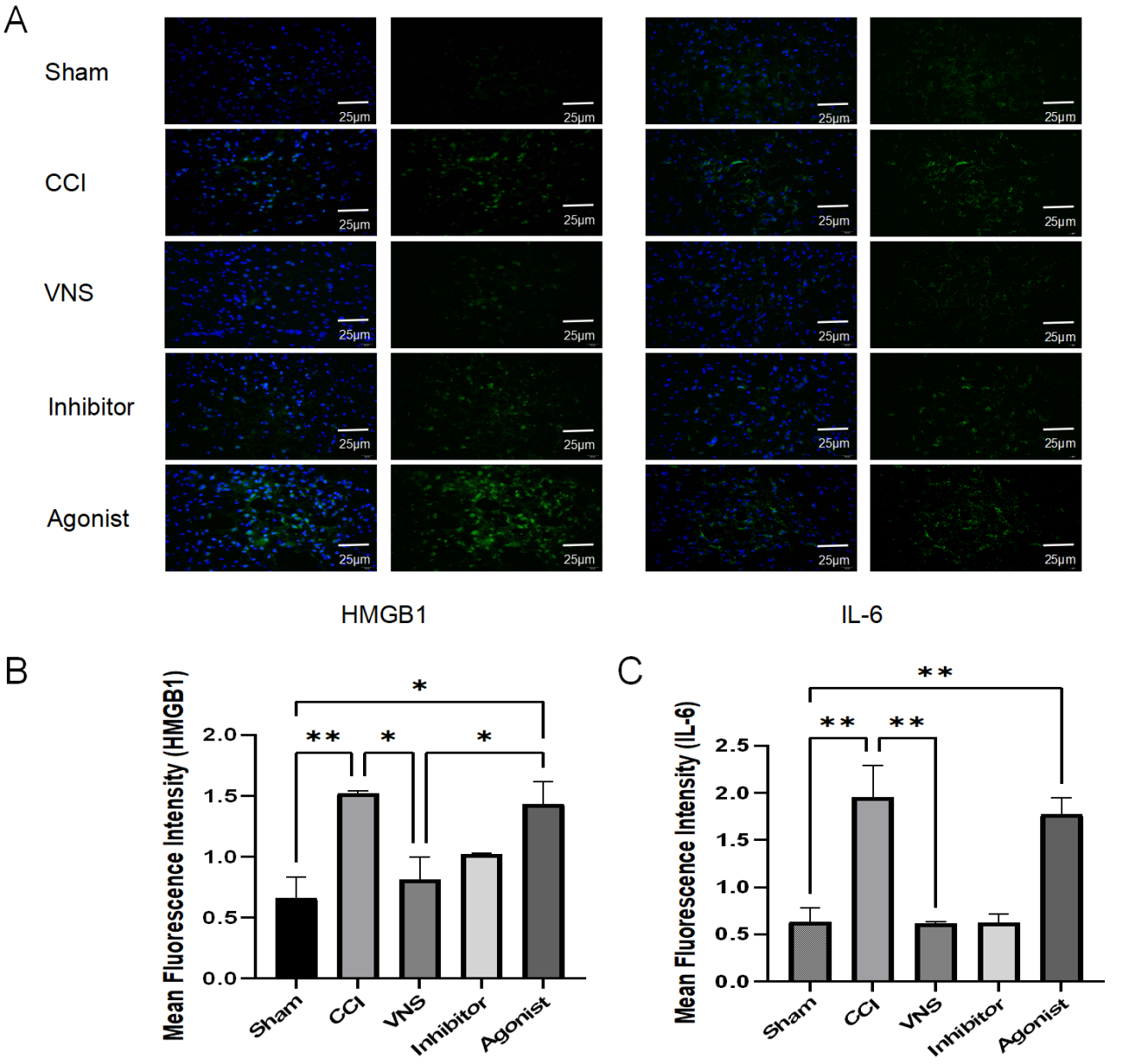

Fig. 5. taVNS suppresses HMGB1 and IL-6 expression in brain tissue post-TBI. (A) Representative immunofluorescence images from the five experimental groups. Cell nuclei were counterstained with 4′,6-diamidino-2-phenylindole (DAPI) (blue). Positive signals for HMGB1 and IL-6 are shown in green. Scale bar = 25 μm. (B,C) Quantitative analysis of the mean fluorescence intensity for (B) HMGB1 and (C) IL-6 in the peri-lesion cortex. Data are presented as mean ± SD. *$p < 0.05$, **$p < 0.01$ (by one-way ANOVA with Tukey's post-hoc test).

ducing the CCI-induced elevation of p-NF-κB p65 and p-ERK1/2 (p-NF-κB p65: $p = 0.001$; p-ERK1/2: $p = 0.0192$). These data provide direct molecular evidence at the level of signaling pathway activation that taVNS exerts its therapeutic anti-edema effect by specifically inhibiting the HMGB1-mediated activation of the NF-κB and MAPK/ERK pathways.

3.4.2 taVNS Suppresses HMGB1 and IL-6 Expression at the Cellular Level

To complement our western blot findings and spatially resolve the expression of key inflammatory mediators, we performed a quantitative analysis of immunofluorescence (IF) images. Consistent with the molecular data, a significant increase in the fluorescence intensity of both HMGB1 and IL-6 was observed in the peri-lesion cortex of the CCI group compared to the Sham group (HMGB1: $p = 0.0084$; IL-6: $p = 0.0045$; Fig. 5B,C). taVNS treatment markedly reduced the signal intensity for both HMGB1 and

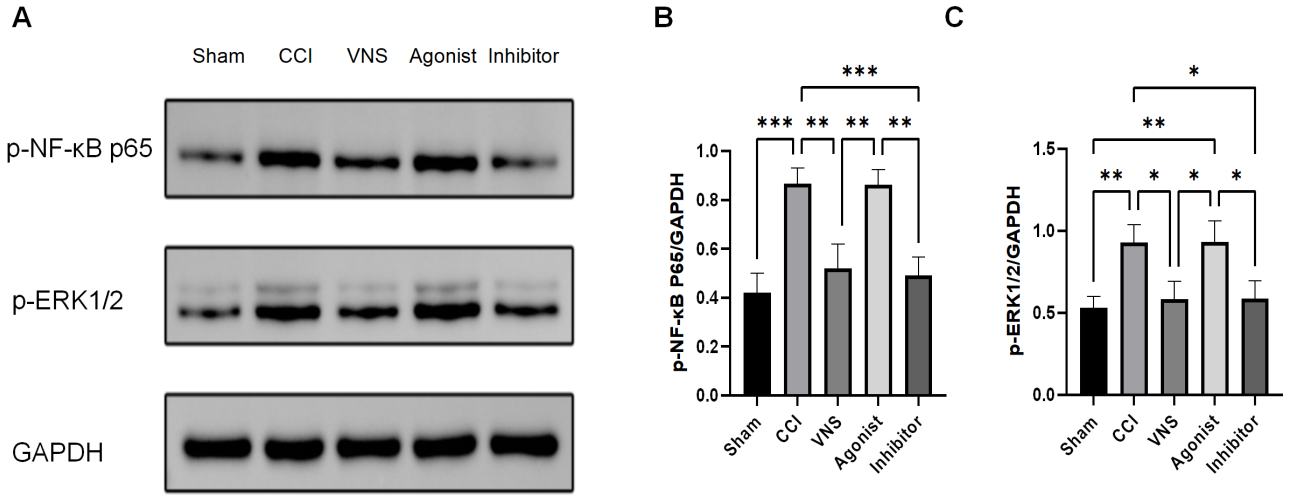

Fig. 6. taVNS suppresses the activation of key downstream effectors in the HMGB1 signaling pathway. (A) Representative western blot images of phosphorylated NF-κB p65 (p-NF-κB p65, Ser536) and phosphorylated ERK1/2 (p-ERK1/2, Thr202/Tyr204) in the brain tissues across the five experimental groups. (B) Quantitative analysis of p-NF-κB p65 protein levels. (C) Quantitative analysis of p-ERK1/2 protein levels. Data are presented as mean $\pm$ SD. *$p < 0.05$, **$p < 0.01$, ***$p < 0.001$ (by one-way ANOVA with Tukey's post-hoc test). NF-κB, nuclear factor kappa-light-chain-enhancer of activated B cells; ERK1/2, extracellular signal-regulated kinase 1/2.

IL-6 compared to the CCI group (HMGB1: $p = 0.0192$; IL-6: $p = 0.0042$). The therapeutic effect of taVNS was abolished by the HMGB1 agonist, as the Agonist group exhibited fluorescence intensity levels comparable to those in the CCI group (HMGB1: $p = 0.9579$; IL-6: $p = 0.8543$). Conversely, monotherapy with the HMGB1 inhibitor mimicked the effect of taVNS, leading to a significant suppression of IL-6 ($p = 0.0043$ vs CCI group) and a strong, albeit non-significant, trend toward reduced HMGB1 ($p = 0.0745$ vs CCI group). Representative IF images are shown in Fig. 5A. These quantitative IF results reinforce the conclusion that taVNS exerts its anti-inflammatory effects by specifically modulating the HMGB1 pathway at the cellular level.

3.4.3 HMGB1 Modulation by taVNS Underlies Functional Recovery and Edema Resolution

To determine whether the therapeutic effects of taVNS specifically on the HMGB1 pathway, this study employed a combined intervention with an agonist (high glucose) and an antagonist (glycyrrhizic acid) at the mechanism level. Behavioral results demonstrated that, by day 10 post-operation, the central area movement distance in the inhibitor group was restored to 69.8% of that in the control group (1648.04 $\pm$ 697.58 cm vs 915.20 $\pm$ 318.59 cm in the CCI group, $p = 0.0317$, Fig. 4A), while the mNSS score decreased to 6.8 $\pm$ 2.3 points (CCI group: 9.10 $\pm$ 2.64 points, $p = 0.0762$, Fig. 4B). In contrast, the Agonist group exhibited a significant reduction in the distance traveled in the center to 39.0% of the control level (896.17 $\pm$ 589.59 cm vs 1648.04 $\pm$ 697.58 cm in the control group) at 10 days. Furthermore, the neurological function of the Agonist group showed no improvement, with mNSS scores of 9.30 $\pm$ 2.26 points, comparable to the CCI group (9.10 $\pm$ 2.64 points) (Fig. 4A,B). Analysis of imaging data revealed that the taVNS group exhibited a 74.7 $\pm$ 12.1% reduction in cerebral volume at 10 days of surgery compared to 3 days of surgery, whereas agonist intervention (TBI + taVNS + high-glucose group) markedly attenuated this effect, reducing absorption to 41.8 $\pm$ 20.6% ($p < 0.0001$ vs taVNS group). This suggests high glucose reverses taVNS regulation by forcibly activating HMGB1. Conversely, HMGB1 inhibition alone (TBI + glycyrrhizic acid group) mimicked the effect of taVNS, achieving a 65.1 $\pm$ 8.7% reduction in edema volume (Fig. 4E). At the molecular level, glycyrrhizic acid alone reduced HMGB1 levels by 10% compared to the trauma group and downstream effector molecules IL-1β and IL-6. Conversely, highsugar these indicators to group levels or higher. HMGB1 (1498.35 $\pm$ 680.69 pg/mL vs 1325.40 $\pm$ 202.64 pg/mL in the injury group) and IL-6 (79.14 $\pm$ 24.48 pg/mL vs 76.16 $\pm$ 10.35 pg/mL) (Fig. 4C) were essentially comparable to those in the trauma group. Protein expression in brain tissue increased to 4.5-fold that of the control group (3.7-fold in the trauma group), while IL-1β levels rose to 3.7-fold that of the control group (2.8-fold in the trauma group) (Fig. 4D). Immunofluorescence revealed the mimetic effect of the inhibitor group on treatment efficacy and the reversal effect of the agonist on treatment efficacy (Fig. 5). This chain of evidence suggests that taVNS specifically affects cerebral and neurological recovery by targeting nuclear translocation and downstream inflammatory cascades. Its effects are mediated by pharmacological agonists and highly mimicked by inhibitors, providing precise mechanistic support for clinical translation.

4. Discussion

TBI encompasses a spectrum of damage resulting from cranial trauma. Beyond its high mortality rate, severe TBI can lead to varying degrees of cognitive impairment and neurological dysfunction, resulting in lifelong disability and imposing substantial economic and health burdens on families and society [12–15]. The primary cause of these sequelae is secondary brain injury; however, effective pharmacological interventions remain limited [16,17]. Following TBI, HMGB1 released from injured cells triggers a cascade of inflammatory mediators, leading to blood-brain barrier (BBB) disruption, neuronal damage, and secondary cerebral edema [18]. This edema is a pivotal pathological mechanism in neurological deterioration. Current clinical management primarily relies on osmotic agents (e.g., mannitol and hypertonic saline) and surgical decompression [19]. However, these measures offer only transient relief from intracranial hypertension without addressing the self-perpetuating cycle of neuroinflammation-driven BBB impairment and glial cell-mediated toxicity.

VNS has attracted interest for its ability to suppress systemic inflammatory responses via activation of the CAP [20]. Nevertheless, conventional invasive VNS requires surgical electrode implantation on the cervical vagus nerve, which limits its clinical applicability due to high costs, impracticality in acute settings, and potential side effects [21]. In contrast, taVNS has emerged as a non-invasive neuromodulation approach. By stimulating the auricular concha region—which corresponds to the "heart" and "brain" acupoints in Traditional Chinese Medicine and is densely innervated by auricular vagal branches—taVNS directly activates the solitary nucleus-locus coeruleus pathway. Animal studies have demonstrated that taVNS exerts anti-inflammatory effects comparable to invasive VNS [22], while avoiding surgical risks and enabling timely intervention. This study aimed to evaluate the role of taVNS in early intervention for post-traumatic cerebral edema and inflammation through targeting HMGB1. Our results indicate that taVNS initiated within 72 hours after TBI significantly enhanced edema resolution (volume reduction rate: 74.7 $\pm$ 12.1% vs spontaneous resolution: 53.5 $\pm$ 16.2%) and exerted marked anti-inflammatory effects. This temporal advantage underscores its unique applicability in early critical care and offers a promising strategy to overcome the "time-window dilemma" associated with conventional VNS.

The release of HMGB1 from necrotic neurons into the extracellular microenvironment following TBI is widely recognized as a central element of the DAMP response. In this study, we employed molecular techniques to assess HMGB1 levels in blood and brain tissue, incorporating interventions such as taVNS, HMGB1 agonists, and inhibitors. Our findings establish that the therapeutic benefits of taVNS are fundamentally associated with modulation of the HMGB1 pathway and its upstream and downstream components. Specifically, high-glucose administration abolished the inhibitory effect of taVNS on HMGB1 and impeded edema resolution, whereas glycyrrhizic acid monotherapy replicated the therapeutic benefits of taVNS. The HMGB1 agonist enhanced the expression of HMGB1 and downstream inflammatory factors in both serum and brain tissue, whereas the antagonist facilitated edema resolution to a certain extent.

Therefore, we propose that taVNS, by attenuating HMGB1 release, disrupts the pro-inflammatory signaling axis, leading to reduced neuroinflammation and subsequent cerebral edema. This conclusion is strongly supported by our novel data showing that taVNS effectively inhibits the activation of NF-κB and ERK, two well-established downstream signaling cascades of HMGB1. The fact that an HMGB1 agonist abolished the suppressive effects of taVNS on these pathways, while an HMGB1 inhibitor replicated them, establishes a direct causal link beyond mere correlation.

This discovery redefines the role of HMGB1 in neuroinflammation: it is not merely a messenger of injury signals, but rather a 'modulable hub' for therapeutic intervention. taVNS may regulate inflammation by modulating HMGB1 levels rather than directly interfering with downstream pathways such as TLR4/NF-κB. This "upstream targeting" characteristic circumvents the immunosuppressive risks associated with broad-spectrum inhibition by conventional anti-inflammatory drugs, offering novel insights for precision medicine. Although the management of post-TBI cerebral edema and elevated intracranial pressure currently relies on hyperosmolar agents such as mannitol and hypertonic saline, these treatments primarily provide transient symptomatic relief by creating an osmotic gradient. A recent meta-analysis of 637 patients demonstrated that while hypertonic saline may offer a longer duration of effect, both agents are largely equivalent in terms of their impact on mortality and long-term neurological outcomes [23]. This underscores a critical limitation of current standard care: it addresses the symptom (edema) without directly targeting the underlying neuroinflammatory pathophysiology that drives its progression. In contrast, our study demonstrates that taVNS intervenes mechanistically at the root of this process by suppressing the HMGB1-initiated inflammatory cascade, thereby not only resolving edema but also actively promoting neurological recovery. This positions taVNS as a paradigm-shifting, non-invasive strategy that moves beyond transient osmotic support towards targeted immunomodulation for secondary brain injury.

In this context, our findings gain significant clinical relevance when contrasted with the current standard of care. The mainstay pharmacological treatment for cerebral edema, glucocorticoids such as dexamethasone, is increasingly recognized for its detrimental immunosuppressive effects, which can antagonize modern immunotherapies and potentially worsen patient outcomes [24]. Our study demonstrates that taVNS achieves comparable anti-

edema efficacy without systemic immunosuppression, positioning it as a promising non-invasive and steroid-sparing alternative for managing neuroinflammation post-TBI.

Furthermore, the trajectory of neurological recovery itself could provide a direct and clinically relevant guide for tailoring treatment length. In this study, the taVNS group demonstrated significantly improved mNSS scores and open field performance by day 11 (Fig. 4A,B). We hypothesize that patients whose functional recovery plateaus or lags behind expectations—as measured by serial assessments using standardized scales such as the extended Glasgow Outcome Scale (GOSE) or mNSS—may represent ideal candidates for an extended course of taVNS. This approach would leverage the treatment's anti-inflammatory and potential pro-repair effects to support ongoing neural repair and plasticity during the critical subacute recovery phase.

Although this study provides valuable insights, several limitations should be acknowledged. First, all experimental subjects were male mice; future studies should include female and aged animals to enhance the generalizability of the findings. Second, although the dry-wet weight method is commonly used to assess cerebral edema, we employed cerebral MRI, which is considered the gold standard for quantitative evaluation. However, this approach is still subject to technical constraints such as partial volume effects at tissue boundaries and significant motion artifacts due to high respiratory rates in rodents (80–120 breaths per minute), which are 3–5 times more pronounced than in humans. Future work could benefit from integrating deep learning-based segmentation and multimodal image registration to improve accuracy. Finally, with regard to stimulation parameters, we used a fixed set of parameters determined during pre-experimental optimization and did not evaluate multiple parameter configurations within the experimental groups. Subsequent investigations should explore parameter optimization and develop adaptive parameter-adjusting systems tailored for multimodal data analysis.

5. Conclusions

taVNS significantly promotes cerebral edema resolution and neurological recovery by specifically inhibiting the HMGB1-mediated inflammatory pathway. Its noninvasive nature and potential for early intervention offer an innovative pathway to overcome therapeutic limitations in secondary brain injury. Future studies should focus on parameter, multiclinical validation, and the development of intelligent devices to advance taVNS from basic research to clinical application, improving long-term outcomes for patients with.

Abbreviations

TBI, traumatic brain injury; CCI, controlled cortical impact; taVNS, transcutaneous auricular vagus nerve stimulation; VNS, vagus nerve stimulation; HMGB1, high mobility group box 1; MAPK, mitogen-activated protein kinase; IL-6, Interleukin-6; IL-1β, Interleukin-1β; mNSS, Modified Neurological Sign Score; SD, Standard deviation; DAPI, 4′,6-diamidino-2-phenylindole.

Availability of Data and Materials

The datasets used and analyzed during the current study are available from the corresponding author on reasonable request.

Author Contributions

YFF and XXL conceived and designed the study. YFF performed the majority of the experiments and data analysis. XXL supervised the project. TJ and CDC contributed to the experimental design, specifically refining the surgical and stimulation protocols, and were solely responsible for the acquisition, processing, and quantitative analysis of all magnetic resonance imaging (MRI) data. MHX performed the statistical analysis and interpreted the behavioral and molecular data. YYC conducted the immunofluorescence experiments and performed quantitative image analysis. JYG and XYX contributed to the study by establishing and optimizing the post-operative animal care protocol, which was critical for ensuring animal welfare and standardized recovery, thereby directly supporting the integrity of the longitudinal data acquisition. SLL contributed to the manuscript by drafting the initial sections on methodology and results, and by participating in the interpretation of the transcriptomic data. All authors participated in revising the manuscript critically for important intellectual content, read, and approved the final version to be published. All authors agree to be accountable for all aspects of the work.

Ethics Approval and Consent to Participate

All experimental procedures were approved by the Ethics Committee of Anhui Medical University (Approval Number: 20252156) and were conducted in accordance with its relevant guidelines and regulations (Guidelines for the Management and Use of Laboratory Animals).

Acknowledgment

The authors would like to thank all colleagues who provided general support and stimulating discussions during the course of this research.

Funding

This research was funded by Anhui University Scientific Research Project, grant number AH2023AH040076.

Conflict of Interest

The authors declare no conflict of interest.

Supplementary Material

Supplementary material associated with this article can be found, in the online version, at https://doi.org/10.31083/JIN47066.

References

[1] Fernández-Gajardo R, Matamala JM, Carrasco R, Gutiérrez R, Melo R, Rodrigo R. Novel therapeutic strategies for traumatic brain injury: acute antioxidant reinforcement. CNS Drugs. 2014; 28: 229–248. https://doi.org/10.1007/s40263-013-0138-y.

[2] Sulhan S, Lyon KA, Shapiro LA, Huang JH. Neuroinflammation and blood-brain barrier disruption following traumatic brain injury: Pathophysiology and potential therapeutic targets. Journal of Neuroscience Research. 2020; 98: 19–28. https://doi.org/10.1002/jnr.24331.

[3] Minchew HM, Ferren SL, Christian SK, Hu J, Keselman P, Brooks WM, *et al*. Comparing imaging biomarkers of cerebral edema after TBI in young adult male and female rats. Brain Research. 2022; 1789: 147945. https://doi.org/10.1016/j.brainres.2022.147945.

[4] Takata F, Nakagawa S, Matsumoto J, Dohgu S. Blood-Brain Barrier Dysfunction Amplifies the Development of Neuroinflammation: Understanding of Cellular Events in Brain Microvascular Endothelial Cells for Prevention and Treatment of BBB Dysfunction. Frontiers in Cellular Neuroscience. 2021; 15: 661838. https://doi.org/10.3389/fncel.2021.661838.

[5] Li M, Lv J, Wang Z, Wang L, Qin Z, Deng C, *et al*. Inhibition of HMGB1 Attenuates Spinal Cord Edema by Reducing the Expression of Na^+-K^+-Cl^- Cotransporter-1 and Na^+/H^+ Exchanger-1 in Both Astrocytes and Endothelial Cells After Spinal Cord Injury in Rats. Journal of Neurotrauma. 2023; 40: 2522–2540. https://doi.org/10.1089/neu.2022.0318.

[6] Ngadimon IW, Mohan D, Shaikh MF, Khoo CS, Tan HJ, Lee YM, *et al*. HMGB1 blood levels and neurological outcomes after traumatic brain injury: Insights from an exploratory study. Epilepsia Open. 2025; 10: 494–507. https://doi.org/10.1002/epi4.70001.

[7] Gao S, Wang D, Liu K, Tomono Y, Fu L, Gao Y, *et al*. Anti-HMGB1 mAb Therapy Reduces Epidural Hematoma Injury. International Journal of Molecular Sciences. 2024; 25: 5889. https://doi.org/10.3390/ijms25115889.

[8] Thompson N, Mastitskaya S, Holder D. Avoiding off-target effects in electrical stimulation of the cervical vagus nerve: Neuroanatomical tracing techniques to study fascicular anatomy of the vagus nerve. Journal of Neuroscience Methods. 2019; 325: 108325. https://doi.org/10.1016/j.jneumeth.2019.108325.

[9] Goggins E, Mitani S, Tanaka S. Clinical perspectives on vagus nerve stimulation: present and future. Clinical Science (London, England: 1979). 2022; 136: 695–709. https://doi.org/10.1042/CS20210507.

[10] Butt MF, Albusoda A, Farmer AD, Aziz Q. The anatomical basis for transcutaneous auricular vagus nerve stimulation. Journal of Anatomy. 2020; 236: 588–611. https://doi.org/10.1111/joa.13122.

[11] Yap JYY, Keatch C, Lambert E, Woods W, Stoddart PR, Kameneva T. Critical Review of Transcutaneous Vagus Nerve Stimulation: Challenges for Translation to Clinical Practice. Frontiers in Neuroscience. 2020; 14: 284. https://doi.org/10.3389/fnins.2020.00284.

[12] Maas AIR, Menon DK, Manley GT, Abrams M, Åkerlund C, Andelic N, *et al*. Traumatic brain injury: progress and challenges in prevention, clinical care, and research. The Lancet. Neurology. 2022; 21: 1004–1060. https://doi.org/10.1016/S1474-4422(22)00309-X.

[13] VanSolkema M, McCann C, Barker-Collo S, Foster A. Attention and Communication Following TBI: Making the Connection through a Meta-Narrative Systematic Review. Neuropsychology Review. 2020; 30: 345–361. https://doi.org/10.1007/s11065-020-09445-5.

[14] Green L, Godfrey C, Soo C, Anderson V, Catroppa C. A preliminary investigation into psychosocial outcome and quality-of-life in adolescents following childhood traumatic brain injury. Brain Injury. 2013; 27: 872–877. https://doi.org/10.3109/02699052.2013.775506.

[15] Fratantoni JM, DeLaRosa BL, Didehbani N, Hart J, Jr, Kraut MA. Electrophysiological Correlates of Word Retrieval in Traumatic Brain Injury. Journal of Neurotrauma. 2017; 34: 1017–1021. https://doi.org/10.1089/neu.2016.4651.

[16] Yan J, Zhang Y, Wang L, Li Z, Tang S, Wang Y, *et al*. TREM2 activation alleviates neural damage via Akt/CREB/BDNF signalling after traumatic brain injury in mice. Journal of Neuroinflammation. 2022; 19: 289. https://doi.org/10.1186/s12974-022-02651-3.

[17] Zhu H, Wang Z, Yu J, Yang X, He F, Liu Z, *et al*. Role and mechanisms of cytokines in the secondary brain injury after intracerebral hemorrhage. Progress in Neurobiology. 2019; 178: 101610. https://doi.org/10.1016/j.pneurobio.2019.03.003.

[18] Alsbrook DL, Di Napoli M, Bhatia K, Biller J, Andalib S, Hinduja A, *et al*. Neuroinflammation in Acute Ischemic and Hemorrhagic Stroke. Current Neurology and Neuroscience Reports. 2023; 23: 407–431. https://doi.org/10.1007/s11910-023-01282-2.

[19] Park M, Shim Y, Choo YH, Kim HS, Kim J, Ha EJ. Should Hypertonic Saline Be Considered for the Treatment of Intracranial Hypertension? A Review of Current Evidence and Clinical Practices. Korean Journal of Neurotrauma. 2024; 20: 146–158. https://doi.org/10.13004/kjnt.2024.20.e35.

[20] Liu FJ, Wu J, Gong LJ, Yang HS, Chen H. Non-invasive vagus nerve stimulation in anti-inflammatory therapy: mechanistic insights and future perspectives. Frontiers in Neuroscience. 2024; 18: 1490300. https://doi.org/10.3389/fnins.2024.1490300.

[21] Bonaz B, Sinniger V, Hoffmann D, Clarençon D, Mathieu N, Dantzer C, *et al*. Chronic vagus nerve stimulation in Crohn's disease: a 6-month follow-up pilot study. Neurogastroenterology and Motility. 2016; 28: 948–953. https://doi.org/10.1111/nmo.12792.

[22] Chen Y, Zhang Y, Wang J, Li S, Wang Y, Zhang Z, *et al*. Anti-neuroinflammation effects of transcutaneous auricular vagus nerve stimulation against depression-like behaviors via hypothalamic α7nAchR/JAK2/STAT3/NF-κB pathway in rats exposed to chronic unpredictable mild stress. CNS Neuroscience & Therapeutics. 2023; 29: 2634–2644. https://doi.org/10.1111/cns.14207.

[23] Karamian A, Seifi A, Lucke-Wold B. Comparing the effects of mannitol and hypertonic saline in severe traumatic brain injury patients with elevated intracranial pressure: a systematic review and meta-analysis. Neurological Research. 2024; 46: 883–892. https://doi.org/10.1080/01616412.2024.2360862.

[24] Goldman M, Lucke-Wold B, Martinez-Sosa M, Katz J, Mehkri Y, Valisno J, *et al*. Steroid utility, immunotherapy, and brain tumor management: an update on conflicting therapies. Exploration of Targeted Anti-tumor Therapy. 2022; 3: 659–675. https://doi.org/10.37349/etat.2022.00106.